Lattice Monte Carlo Simulations of Phase Separation and Micellization in Supercritical CO_2/Surfactant Systems: Effect of CO_2 Density

Lauriane F. Scanu, Keith E. Gubbins, and Carol K. Hall*

Department of Chemical Engineering, North Carolina State University, Raleigh, North Carolina 27695-7905

Received May 6, 2003. In Final Form: October 3, 2003

Lattice Monte Carlo simulations are used to study the effect of nonionic surfactant concentration and CO_2 density on the micellization and phase equilibria of supercritical CO_2/surfactant systems. The interaction parameter for carbon dioxide is obtained by matching the critical temperature of the model fluid with the experimental critical temperature. Various properties such as the critical micelle concentration and the size, shape, and structure of micelles are calculated, and the phase diagram in the surfactant concentration−CO_2 density space is constructed. On increasing the CO_2 density, we find an increase in the critical micelle concentration and a decrease in the micellar size; this is consistent with existing experimental results. The variation of the micellar shape and structure with CO_2 density shows that the micelles are spherical and that the extension of the micellar core increases with increasing micellar size, while the extension of the micellar corona increases with increasing CO_2 density. The predicted phase diagram is in qualitative agreement with experimental phase diagrams for nonionic surfactants in carbon dioxide.

I. Introduction

The behavior of surfactants in critical and supercritical carbon dioxide has received considerable attention in recent years due to the opening up of new application areas for CO_2 as a green solvent.[1−5] CO_2 has many attractive features in this regard. It is environmentally benign, inexpensive, nontoxic, and readily available. Additionally, its solvating ability can be tuned by varying pressure and/or temperature. Paradoxically, dense CO_2 is a very poor solvent for many organic substances because it is nonpolar and has weak van der Waals forces. However, this limitation can be circumvented by the addition of surfactants[6,7] that contain a CO_2-philic tail which dissolves in the bulk solvent and a CO_2-phobic head which avoids the CO_2. When a sufficient number of surfactant molecules are present in CO_2, they form micelles that can solubilize CO_2-phobic molecules within their core, a phenomenon known as micellar solubilization.

While surfactants have greatly enhanced the utility of carbon dioxide, our understanding of their behavior in solution is still essentially a work in progress. To date, studies of surfactant phase behavior and micellization in supercritical carbon dioxide are mainly experimental;[8−11] only a few are computational. Lisal et al.[12,13] performed canonical lattice Monte Carlo simulations to study the effect of surfactant architecture on the micellar behavior of perfluoroalkylpoly(ethylene oxide) in supercritical carbon dioxide. A pseudophase diagram showing micellar and unimer phases in the CO_2 density−surfactant concentration plane was constructed for several surfactant architectures. The critical micelle concentration was found to decrease with increasing CO_2 density and surfactant head length; the former result is the opposite of that found in experiments. Lisal et al. also looked at the solubilization of water molecules by using a two-box simulation method. They found that at low water concentration, the water molecules are solubilized throughout the surfactant head region, while at high water concentration, the water molecules are also solubilized in the micelle center as a water core. Senapati et al.[14] used molecular dynamics simulations to study the shape and structure of a micelle in a CO_2/dichain surfactant/water system and compared their results with small-angle neutron scattering experiments. Their simulated reverse micelle was slightly

(1) DeSimone, J. M.; Guan Z.; Elsbernd C. S. Synthesis of fluoropolymers in supercritical carbon dioxide. *Science* **1992**, *257* (5072), 945−947.

(2) McHugh, M. A.; Krukonis, V. J. *Supercritical Fluid Extraction*: *Principles and Practice*, 2nd ed.; Butterworth-Heinemann: Boston, 1994.

(3) Shim, J.-J.; Yates, M. Z.; Johnston, K. P. Polymer Coatings by Rapid Expansion of Suspensions in Supercritical Carbon Dioxide. *Ind. Eng. Chem. Res.* **1999**, *38* (10), 3655−3662.

(4) DeSimone, J. M.; Maury, E. E.; Menceloglu, Y. Z.; McClain, J. B.; Romack, T. J.; Combes, J. R. Dispersion polymerizations in supercritical carbon dioxide. *Science* **1994**, *265* (5170), 356−359.

(5) Henon, F. E.; Camaiti, M.; Burke, A. L. C.; Carbonell, R. G.; DeSimone, J. M.; Piacenti, F. Supercritical CO_2 as a solvent for polymeric stone protective materials. *J. Supercrit. Fluids* **1999**, *15* (2), 173−179.

(6) Jimenez-Carmona, M. M.; Luque de Castro, M. D. Reverse-micelle formation: a strategy for enhancing CO_2-supercritical fluid extraction of polar analytes. *Anal. Chim. Acta* **1998**, *358* (1), 1−4.

(7) Goetheer E. L. V.; Vorstman M. A. G.; Keurentjes, J. T. F. Opportunities for process intensification using reverse micelles in liquid and supercritical carbon dioxide. *Chem. Eng. Sci.* **1999**, *54* (10), 1589−1596.

(8) DeSimone, J. M.; Keiper, J. S. Surfactants and self-assembly in carbon dioxide. *Curr. Opin. Solid State Mater. Sci.* **2001**, *5* (4), 333−341.

(9) Hoefling, T. A.; Beitle, R. R.; Enick, R. M.; Beckman, E. J. Design and synthesis of highly carbon dioxide-soluble surfactants and chelating agents. *Fluid Phase Equilib.* **1993**, *83*, 203−212.

(10) O'Neill, M. L.; Cao, Q.; Fang, M.; Johnston, K. P.; Wilkinson, S. P.; Smith, C. D.; Kerschner, J. L.; Jureller, S. H. Solubility of Homopolymers and Copolymers in Carbon Dioxide. *Ind. Eng. Chem. Res.* **1998**, 37 (8), 3067−3079.

(11) McClain, J. B.; Betts, D. E.; Canelas, D. A.; Samulski, E. T.; DeSimone, J. M.; Londono, J. D.; Cochran, H. D.; Wignall, G. D.; Chillura-Martino, D.; Triolo, R. Design of nonionic surfactants for supercritical carbon dioxide. *Science* **1996**, *274* (5295), 2049−2051.

(12) Lisal, M.; Hall, C. K.; Gubbins, K. E.; Panagiotopoulos, A. Z. Self-assembly of surfactants in a supercritical solvent from lattice Monte Carlo simulations. *J.* Chem. Phys. **2002**, *116* (3), 1171−1184.

(13) Lisal, M.; Hall, C. K.; Gubbins, K. E.; Panagiotopoulos, A. Z. Micellar behavior in a supercritical solvent-surfactant from lattice Monte Carlo simulations. *Fluid Phase Equilib.* **2002**, *194*, 233−247.

(14) Senapati, S.; Keiper, J. S.; DeSimone, J. M.; Wignall G. D.; Melnichenko, Y. B.; Frielinghaus, H.; Berkowitz, M. L. Structure of Phosphate Fluorosurfactant Based Reverse Micelles in Supercritical Carbon Dioxide. *Langmuir* **2002**, *18* (20), 7371−7376.

10.1021/la0347760 CCC: $27.50
Published on Web 12/20/2003

elongated and stable over a time period of 4 ns. The radius of gyration and the area per surfactant head determined via simulation were in good agreement with experimental results. Salaniwal et al.[15,16] performed molecular dynamics simulations of the self-assembly and structural properties of surfactant aggreates in a water/dichain anionic surfactant/carbon dioxide system. They showed that micellization is a two-step process that consists of the rapid hydration of the surfactant headgroups and then slow aggregation of the hydrated surfactant heads through hydrogen bonding. They also noted that as the fluorination of the surfactant tail increases, micellization becomes slower. The surfactant tail length did not affect the kinetics of this process. Colina et al.[17] used the statistical associating fluid theory to predict the phase behavior of PVAC-*b*-PTAN in CO_2. They found good agreement with experimental results on the PVAC/CO_2, PTAN/CO_2, and PVAC-*b*-PTAN/CO_2 cloud curves and on the PVAC-*b*-PTAN/CO_2 critical micellar densities.

Computational studies aimed at understanding surfactant phase behavior and micellization in solvents other than CO_2 represent a more extended literature. Here, we briefly review those based in lattice Monte Carlo. A more complete review can be found in Shelley and Shelley.[18] Off-lattice Monte Carlo and molecular dynamics (MD) studies are limited to system sizes of about 5−10 nm and (for MD) to real times of the order of a few nanoseconds, too small and too short, respectively, to study micellization. Lattice Monte Carlo methods permit system sizes of 100 nm or more to be studied, making it possible to calculate phase behavior and micelle structures over a wide range of densities, temperatures, and concentrations.

Lattice Monte Carlo simulations were first used to study surfactant/oil/water systems by Larson et al.[19] in 1985. Since Larson's model is essentially the basis of our study, it is appropriate to describe it and follow-on studies in somewhat more detail. The model consists of a fully occupied cubic lattice in which each site interacts equally with all 26 neighbors. Each site can be either an oil molecule, a water molecule, or a surfactant unit. The surfactant molecule, denoted by H_iT_j, contains *i* head units (H) and *j* tail units (T). The model is characterized by one dimensionless energy parameter, *w*, which describes the difference in interaction energies between solvophilic and solvophobic units. Surfactant molecules are moved using chain twisting and reptation, while water and oil molecules are interchanged. During the past decade, Panagiotopoulos and co-workers extended Larson's model by applying Gibbs ensemble methodology[20] to determine phase equilibria and histogram-reweighting grand canonical MC methodology[21] to study micellization processes. They also implemented new moves such as surfactant regrowth[22] by using the configurational bias MC method and cluster moves[23] to displace entire micelles by one site.

Lattice-based Monte Carlo simulations have been used[19−38] extensively by many other investigators because of their computational efficiency. Although they require coarse graining of intermolecular interactions and molecular architecture, they have provided considerable insight into phase transitions and aggregation phenomena for surfactants in incompressible systems. Ternary phase diagrams and ordered phase structures (including micellar, hexagonal, lamellar and cubic) for water/surfactant/oil modeled systems have been calculated for several surfactant architectures[19,22,27] as a function of temperature,[25,26,32] surfactant head/tail ratio,[22,26,32] and concentration.[24,26,33] Binary phase diagrams, critical micelle concentration, and micelle characterizations (such as size, shape, and structure) for surfactant/solvent systems have also been determined for several surfactant architectures as a function of temperature,[21,28,29,34,35] surfactant head/tail ratio[30,31,34−36] and concentration,[23,28,36] and interaction energies.[28,37,38] As we will see, lattice-based Monte Carlo simulations are also capable of predicting experimental trends and of providing a wealth of information on the effect of CO_2 density on solvent quality.

In this paper, we report the results of lattice Monte Carlo simulations of phase behavior and micellization in supercritical CO_2/surfactant systems. Our model surfactant is composed of four CO_2-phobic head sites and five CO_2-philic tail sites. A single site represents the CO_2

(15) Salaniwal, S.; Cui S. T.; Cummings, P. T.; Cochran, H. D. Self-Assembly of Reverse Micelles in Water/Surfactant/Carbon Dioxide Systems by Molecular Simulation. *Langmuir* **1999**, *15* (16), 5188−5192.
(16) Salaniwal, S.; Cui, S.; Cochran, H. D.; Cummings, P. T. Molecular Dynamics Simulation of Reverse Micelles in Supercritical Carbon Dioxide. *Ind. Eng. Chem. Res.* **2000**, *39* (12), 4543−4554.
(17) Colina, C. M.; Hall, C. K.; Gubbins, K. E. Phase behavior of PVAC−PTAN block copolymer in supercritical carbon dioxide using SAFT. *Fluid Phase Equilib.* **2002**, *194*−197, 553−565.
(18) Shelley, J. C.; Shelley, M. Y. Computer simulation of surfactant solutions. *Curr. Opin. Colloid Interface Sci.* **2000**, *5*, 101−110.
(19) Larson, R. G.; Scriven, L. E.; Davis, H. T. Monte Carlo simulation of model amphiphile-oil-water systems. *J.* Chem. Phys. **1985**, *83*, 2411−2420.
(20) Mackie, A. D.; O'Toole, E. M.; Hammer, D. A.; Panagiotopoulos, A. Z. Molecular simulation of self-assembly in surfactant and proteins solutions. *Fluid Phase Equilib.* **1993**, *82*, 237−249.
(21) Floriano, M. A.; Caponetti, E.; Panagiotopoulos, A. Z. Micellization in Model Surfactant Systems. *Langmuir* **1999**, *15* (9), 3143−3151.
(22) Mackie, A. D.; Onur, K.; Panagiotopoulos, A. Z. Phase equilibria of a lattice model for an oil−water-amphiphile mixture. *J. Chem. Phys.* **1996**, *104* (10), 3718−3725.
(23) Mackie, A. D.; Panagiotopoulos, A. Z.; Szleifer, I. Aggregation behavior of a lattice model for amphiphiles. *Langmuir* **1997**, *13*, 5022−5031.
(24) Larson, R. G. Monte Carlo lattice simulation of amphiphilic systems in two and three dimensions. *J. Chem. Phys.* **1988**, *89* (3), 1642−1650.
(25) Larson, R. G. Self-assembly of surfactant liquid crystalline phases by Monte Carlo simulation. *J. Chem. Phys.* **1989**, *91* (4), 2479−2488.
(26) Larson, R. G. Monte Carlo simulation of microstructural transitions in surfactant systems. *J.* Chem. Phys. **1992**, *96*, 7904−7918.
(27) Larson, R. G. Monte Carlo simulations of the Phase Behavior of Surfactant Solutions. *J. Phys. II* **1996**, *6*, 1441−1463.
(28) Desplat, J. C.; Care, C. M. A Monte Carlo simulation of the micellar phase of an amphiphile and solvent mixture. *Mol.* Phys. **1996**, *87* (2), 441−453.
(29) Nelson, P. H.; Rutledge G. C.; Hatton, T. A. On the size and shape of self-assembled micelles. *J. Chem. Phys.* **1997**, *107* (24), 10777−10781.
(30) Rodriguez-Guadarrama, L. A.; Talsania, S. K.; Mohanty, K. K.; Rajagopalan, R. Thermodynamics of Aggregation of Amphiphiles in Solution from Lattice Monte Carlo Simulations. *Langmuir* **1999**, *15* (2), 437−446.
(31) Panagiotopoulos, A. Z.; Floriano, M. A.; Kumar, S. K. Micellization and phase separation of diblock and triblock model surfactants. *Langmuir* **2002**, *18* (7), 2940−2948.
(32) Larson, R. G. Molecular simulation of ordered amphiphilic phases. *Chem.* Eng. Sci. **1994**, *49* (17), 2833−2850.
(33) Laradji, M.; Guo, H.; Zuckermann, M. J. A triangular lattice model for binary and ternary mixtures containing surfactants. *J.* Phys.: *Condens. Matter* **1994**, *6*, 2799−2812.
(34) Bhattacharya, A.; Mahanti, S. D. Critical micelle concentration in three-dimensional lattice models of amphiphiles. *J. Phys.*: *Condens. Matter* **2001**, *13* (41), L861−869.
(35) Kenward, M.; Whitmore, M. D. A systematic Monte Carlo study of self-assembling amphiphiles in solution. *J. Chem. Phys.* **2002**, *116* (8), 3455−3470.
(36) Talsania, S. K.; Wang, Y.; Rajagopalan, R.; Mohanty, K. K. Monte Carlo simulations for micellar encapsulation. *J. Colloid Interface Sci.* **1997**, *190*, 92−103.
(37) Talsania, S. K.; Rodriguez-Guadarrama, L. A.; Mohanty, K. K.; Rajagopalan, R. Phase Behavior and Solubilization in Surfactant-Solute−Solvent Systems by Monte Carlo Simulations. *Langmuir* **1998**, *14* (10), 2684−2692.
(38) Viduna, D.; Milchev, A.; Binder, K. Monte Carlo simulation of micelle formation in block copolymer solutions. *Macromol. Theory Simul.* **1998**, *7*, 649−658.

molecule, and vacancies are included to account for the compressibility of such systems. We have performed simulations at surfactant mole fractions $X_S = 0.002$, 0.0035, 0.005, and 0.0065, and CO_2 reduced densities $\rho_r = 1.3$, 1.4, 1.5, 1.6, 1.7, and 1.8. The free surfactant mole fraction, micelle size distribution, radii of gyration, density profile within the micelle, and micelle−micelle contact factor have been monitored to determine the system's equilibrium properties including the critical micelle concentration (cmc) and the size, shape, and structure of the micelles.

Highlights of our results are the following. At constant CO_2 density, the micelle size remains constant and the mole fraction of surfactants forming micelles increases as the surfactant concentration increases. The micelles are found to be spherical. These results are consistent with other simulations studies and experimental trends. The phase diagram in the surfactant concentration−CO_2 density space is constructed. Three regions are distinguished: a two-phase region at low CO_2 density, a free surfactant region at high CO_2 density and low surfactant concentration, and a micellar region at high CO_2 density and high surfactant concentration. We find an increase in the cmc and a decrease in the micellar size with increasing CO_2 density, consistent with experiments. The micellar structure, described by plotting the density profile within a micelle, shows two regions: (1) a micellar core containing surfactant heads and CO_2 sites whose density increases with increasing distance from the micelle center of mass and (2) a micellar corona consisting of surfactant tails highly solvated by CO_2. Calculation of the radii of gyration for the micelle and for the micellar core gives information not only on the micellar shape but also on the variation of the micellar core and corona extension with increasing CO_2 density. The micelles are found to be spherical. The extension of the micellar core increases with increasing micellar size, while the extension of the micellar corona increases with increasing CO_2 density.

The remainder of this paper is organized as follows: Section II presents the details of the lattice Monte Carlo model and simulation method used in this study. Section III reports our results on the effect of surfactant concentration on the size, shape, and structure of micelles at constant CO_2 density. The phase diagram in the surfactant concentration−CO_2 density space is described and the effect of CO_2 density on the size, shape, and structure of micelles is also reported. Finally, we conclude the paper in section IV with a brief summary of our findings.

II. Methodology

II.1. Model. In the model used here, originally proposed by Larson,[19,24,25] three-dimensional space is discretized by dividing it into a cubic lattice of sites. Solvent molecules (C) occupy a single site, while surfactant molecules (S), denoted by H_mT_n, consisting of m hydrophilic head units, H, and n CO_2-philic tail units, T, occupy $r = m + n$ connected sites. Solvent molecules, surfactant head units, and surfactant tail units interact with equal magnitude with nearest and next-nearest neighbors at $(x,y,z) = (0,0,1)$, $(0,1,1,)$, $(1,1,1)$ plus all vectors resulting from symmetry operations along the x, y, and z axes. The corresponding coordination number for the lattice is $z = 26$. The r sites of the surfactant molecule can be connected along any of these 26 vectors.

The systems studied here are designed to mimic binary mixtures of supercritical CO_2 and nonionic surfactant (scC/S). As suggested by Lisal et al.,[12] the lattice is not fully occupied but contains vacancies (V) in order to account for the compressibility of such systems. Assuming that solvent molecules, surfactant head units, and surfactant tail units are all of the same size, these authors estimated the volume of a lattice site[13] to be $v^* = 78.145$ Å^3. Consequently, the box volume, i.e., the total volume of the system, is $V_T = (N_C + rN_S + N_v)^* v^*$, where N_C is the number of CO_2 molecules, N_S the number of surfactant molecules, and N_v the number of vacant sites. The CO_2 density in the box is defined to be $\rho_{sim}^{CO_2} = N_C/V_T$, where V_T is the total box volume. However, in what follows, it is more convenient to characterize the system according to the CO_2 reduced density, $\rho_r = \rho_{sim}^{CO_2}/\rho_C^{CO_2}$, where $\rho_C^{CO_2}$ is the experimental value of the critical CO_2 density (10636 mol·m^{-3}). The surfactant concentration is defined in terms of the mole fraction, i.e., $X_S = N_S/(N_S + N_C)$.

II.2. Interaction Energies. Many different methods have been used to set up the molecular interaction parameters in Monte Carlo simulations of incompressible binary and ternary surfactant systems.[19,21−38] The simplest ones describe the system with a single dimensionless interaction energy parameter $w = \epsilon/kT = \epsilon_{ij} - 1/2(\epsilon_{ii} + \epsilon_{jj})$, where k is Boltzmann's constant, T is the temperature, i and j are two components of the system (head, tail, solvent, and/or solute), and the ϵ_{ij} are the interaction energies between components i and j. Following Larson et al.,[19,24−27] Mackie et al.[22,23] chose i and j to be the solvophilic (head and water) and solvophobic (tail and oil) components, respectively. Thus, two components that are of the same kind, say solvophilic (head and water sites), are assumed to interact as if they were identical to each other. Additionally, ϵ_{ii} and ϵ_{jj} were assumed to be zero. With this choice of interaction energies, the dimensionless parameter w is ϵ_{ij}/kT. Others investigators have set values for some interaction energies and have taken all the other interactions to be zero. For example, some authors specify repulsive interaction energies between head and tail sites and between water and tail sites,[29,30] while other investigators consider a single attractive interaction energy between two tail sites[21,31] or a mixture of attractive and repulsive interaction energies.[35,36]

Our system differs from the systems discussed above in two respects. First, vacancies are included in the model to account for the system compressibility but do not interact with the molecular components, i.e., $\epsilon_{iv} = 0$. This means that none of the molecular components in the system can have their interaction energies set equal to 0 because then they would be no different than a vacancy. Therefore, the parameter sets described previously cannot be used, i.e., all of the interaction energies ϵ_{ij} with $i, j \neq v$ must have a value different from 0. Second, the solvent−solvent interaction energy needs to be chosen so that we are certain that we are performing simulations in the carbon dioxide supercritical region. This interaction energy can be estimated by matching the critical temperature of the model fluid with the critical temperature of the real fluid, giving $\epsilon_{CC}/k_B = -52$ K, where k_B is Boltzmann's constant.[12] All the other interaction energies ϵ_{ij} (i, j = C, H, T) are then given a value relative to $\epsilon \equiv |\epsilon_{CC}/k_B|$. For the sake of simplicity, the dimensionless interaction energy parameters $w_{ij} = \epsilon_{ij} - 1/2(\epsilon_{ii} + \epsilon_{jj})$ for CO_2-phobic interactions, w_{CH} and w_{HT} are set equal to $+1\epsilon$ and for CO_2-philic interactions, w_{CT} is set equal to -2ϵ. Justification for this set of parameters is the following. The repulsive interactions (w_{CH} and w_{HT}) are known to be important in the force balance driving micellization;[37] a mild repulsion is chosen to ensure that the cmc does not occur at a surfactant concentration that is too low. In contrast, w_{CT} is chosen to be very attractive because the CO_2-philic interaction (ϵ_{CT}) plays an important role in

Table 1. Interaction Energies and Energy Parameters for the Lattice Model of H_4T_5 Surfactant in Supercritical CO_2 (T = 330 K, $\epsilon \equiv |\epsilon_{CC}/k_B|$ = 52 K, k_B Is Boltzmann's Constant)

type of interaction	ϵ_{ii}/k_B (K)	type of interaction	ϵ_{ij}/k_B (K)	w_{ij}
CO_2-CO_2	$-\epsilon$	CO_2−tail	-3ϵ	-2ϵ
tail−tail	$-\epsilon$	CO_2−head	$-\epsilon$	$+1\epsilon$
head−head	-3ϵ	tail−head	$-\epsilon$	$+1\epsilon$

rendering the surfactant soluble in CO_2. Table 1 summarizes the values of the interaction energies, ϵ_{ij}, and energy parameters, w_{ij}, between the molecular components in the system.

II.3. Simulation Details. Micelle formation, or micellization, occurs at a surfactant concentration called the critical micelle concentration (cmc). To ensure that the micelles formed are typical of the solution in the thermodynamic limit of infinite system size, the simulation box must be large enough to observe 5 to 10 micelles.[23] Thus, we use large-scale canonical (NVT) simulations with lattice sizes ranging from 40^3 (for higher surfactant concentrations and system densities) up to 120^3 (for lower surfactant concentrations and system densities). Periodic boundary conditions are employed in all dimensions.

In Larson's original work,[19] reptation moves were used for the surfactant molecules and switch moves were used for the oil and water sites. In this work, reptation moves are maintained and switch moves are used for the solvent and vacancy sites. Additionally, we use the configurational-bias sampling method[39,40] to remove a random chain (or part of it) and regrow it in a different location. We do not perform cluster moves,[21,23,31] in which the whole micelle is shifted by one site in a random direction, because of their high computational cost. Cluster moves are performed to achieve significant micelle displacement. However, an animation of a typical system containing micelles shows that in the absence of cluster moves the micelles explore the entire simulation box space during the course of a simulation.

Following standard practice, we start each NVT MC simulation from a random configuration. Each simulation cycle consists of rN_S attempts to move a randomly chosen surfactant molecule and rN_S attempts to move a randomly chosen solvent molecule. In the case of a surfactant molecule move, reptation or configurational bias is selected randomly with the same probability. A typical MC run is divided into 1.5×10^5 to 2.0×10^5 cycles for equilibration and 5×10^5 to 8×10^5 cycles for evaluation of quantities of interest.

II.4. Characterization Methods. Quantities such as the free surfactant mole fraction, the aggregation number, the radii of gyration, and the density profile within a micelle are monitored during the simulation to characterize the system. These data is then used to calculate properties such as the cmc and the size, shape, and structure of the micelles. Additionally, we evaluate the micelle−micelle contact factor which is a measure of the extent to which the micelles pack together at low CO_2 density when the surfactants phase separate from CO_2. The sampled quantities and the resulting properties are defined below.

Critical Micelle Concentration. It is well-known that when a surfactant solution reaches a specific concentration, called the critical micelle concentration (cmc), the surfactant molecules self-assemble into an aggregate called a micelle. Even though the term "micelle" is formally used for aggregates formed in polar solvents and the term "reverse micelle" is used for aggregates formed in nonpolar solvents, we will refer to our aggregates as micelles for the sake of convenience. A surfactant chain is considered to belong to a micelle if at least one head unit has a nearest or next-nearest-neighbor contact with a head unit from another surfactant chain. Free surfactants are those that are not part of a micelle. There are several ways to define the critical micelle concentration.[21,31,41,42] We define it here as the total surfactant concentration at which half of the surfactant molecules participate in micelles, while the other half remain individually solubilized.[43] A typical plot of the free surfactant mole fraction (X_S^f) versus the total surfactant mole fraction (X_S) is shown in Figure 1. According to our definition, the cmc is the concentration at which the straight line through the simulation results and the straight line through the origin with a slope of 0.5 intersect. The former (solid) line corresponds to the free surfactant concentration and the latter (dashed) line to half of the total surfactant concentration. For example on this plot, the cmc for H_4T_5 surfactant in supercritical CO_2 at $\rho_r = 1.8$ and $T = 330$ K is $X_{cmc} = 0.00215$. To determine the cmc, we typically perform four simulations in the micellar region varying X_S from 0.002 up to 0.0065.

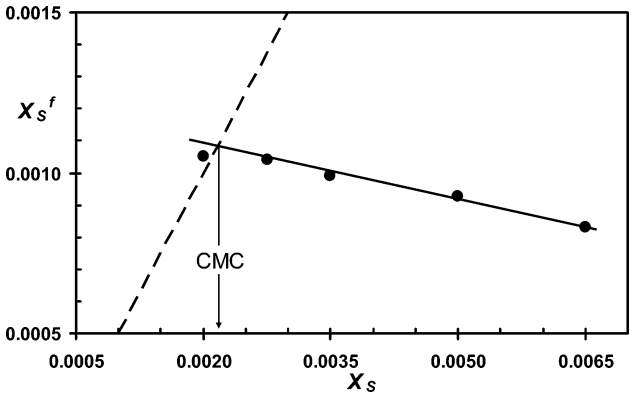

Figure 1. Mole fraction of free surfactant (X_S^f) vs mole fraction of total surfactant (X_S) for H_4T_5 at CO_2 reduced density $\rho_r = 1.8$ and $T = 330$ K. The dashed line corresponds to $X_S^f = X_S/2$ and the solid line is fit to simulation results (●). Statistical uncertainties are smaller than the symbol size.

Micellar Size. The number of surfactant chains in a micelle, also called the aggregation number, n, characterizes the size of the micelle. However, since micelles are dynamic entities with surfactant chains entering and leaving constantly, they have a distribution of aggregation numbers. The mean aggregation number N_a is defined to be

$$N_a = \sum_{n>5} nN_n / \sum_{n>5} N_n$$

where N_n is the number of micelles with aggregation number n. Note that free surfactant ($n = 1$) and small aggregates ($2 \le n \le 5$) are not used in the calculation of N_a. We also define the mole fraction of surfactants in a

(39) Siepmann, J.; Frenkel, D. Configurational bias Monte Carlo: a new sampling scheme for flexible chains. *Mol. Phys.* **1992**, *75*, 59−70.
(40) Rosenbluth, M. N.; Rosenbluth, A. W. Monte Carlo calculation of the average extension of molecular chains. *J. Chem. Phys.* **1955**, *23*, 356−359.
(41) Tanford, C. *The hydrophobic effect*: *formation of micelles and biological membranes*; Wiley: New York, 1980.
(42) Ruckenstein, E.; Nagajaran, R. Critical Micelle Concentration. A transition Point for Micellar Size Distribution. *J. Phys. Chem.* **1975**, *79* (24), 2622−2626.
(43) Israelachvili, J. N.; Mitchell, D. J.; Ninham, B. W. Theory of self-assembly of hydrocarbon amphiphiles into micelles and bilayers. *J. Chem. Soc., Faraday Trans.* **1976**, *2* (72), 1525−1568.

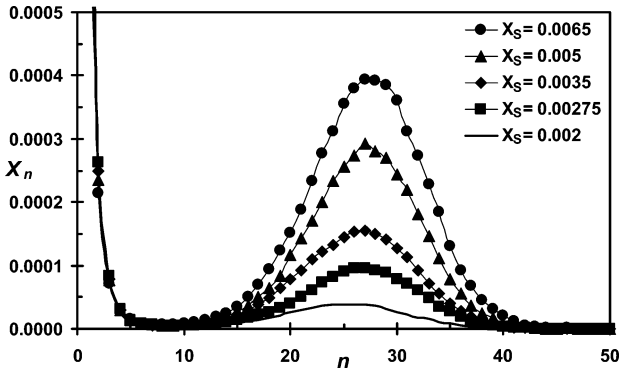

Figure 2. Mole fraction of surfactants in an aggregate of size n (X_n) vs aggregation number (n) for H_4T_5 at $\rho_r = 1.8$, $T = 330$ K, and five surfactant mole fractions (X_S).

size n aggregate, X_n, so that the sum of these mole fractions over all n is equal to the overall surfactant mole fraction i.e., $\sum_{n=1} X_n = X_S$. For $n = 1$, the mole fraction of surfactants is equal to the free surfactant mole fraction, i.e., $X_{(n=1)} = X_S^f$.

Typical sets of aggregate size distributions are shown in Figure 2, which depicts the mole fraction of surfactants in an aggregate of size n vs the aggregation number at five concentrations. At low aggregation number, typically $n \leq 5$, the distribution is a monotonically decreasing function of n, indicating the presence of free surfactants and small aggregates. The peak observed at higher aggregation numbers corresponds to micelles and is generally referred to as the micellar peak. As seen in Figure 2, the distribution is clearly bimodal and the micellar peak is very well defined. Hence, in these and similar cases, we can calculate the mole fraction of surfactants in micelles in the simulation box, X_{mic}, by determining the area under the micellar peak. For ease of comparison, we also report the percentage of surfactants forming micelles, P_{mic}, defined to be

$$P_{mic} = (X_{mic}/X_S) \times 100$$

Micellar Shape. The determination of micellar shape is not as precise as the determination of micellar size since there is no one, well-defined numerical measure that can be used to represent all shapes. The best measure of the micellar shape is the radius of gyration tensor.[13,14,23,26,29,36,44] This quantity is calculated by using the following expression

$$R_{\gamma\delta}{}^2 = \frac{1}{N_{site}} \sum_{i=1}^{N_{site}} (\gamma_i - \gamma_{cm})(\delta_i - \delta_{cm})$$

where γ_i and δ_i are the x,y,z coordinates of surfactant site i on the micelle, the subscript cm stands for the center of mass of the micelle, and N_{site} is the total number of surfactant sites in the micelle. The three eigenvalues of the tensor are called the principal radii of gyration (R_1, R_2, and R_3). These are averaged over all micelles during the course of a simulation. For a perfectly spherical micelle, the three radii of gyration are all equal. As the micellar shape changes from spherical to elongated and cylindrical, R_3 increases to infinity while $R_1 = R_2 < \infty$. Another useful quantification of the micellar shape is the asphericity parameter defined by

$$\alpha_S = \frac{(R_1 - R_2)^2 + (R_1 - R_3)^2 + (R_2 - R_3)^2}{2(R_1 + R_2 + R_3)^2}$$

The asphericity parameter is equal to zero for a perfectly spherical micelle, increases for an elongated micelle, and reaches a maximum of 1 for a cylindrical micelle. Conventionally, a micelle is considered spherical if $\alpha_S \leq 0.1$.[44] In addition to determining the conventional radii of gyration, we also determine the three radii of gyration for the micellar core[14] (R_{c1}, R_{c2}, and R_{c3}) whose outer boundary is the interface between the surfactant heads and tails, also called the core−corona interface. For spherical micelles, we can calculate the mean radii of gyration for the micelle, R, and for the micellar core, R_c, defined by

$$R = (R_1 + R_2 + R_3)/3$$

and

$$R_c = (R_{c1} + R_{c2} + R_{c3})/3$$

The difference between the mean radius of gyration for the micelle and the mean radius of gyration for the micellar core gives us information about how far the surfactant tail is extended into the solvent, i.e., the extent of the micellar corona.

Density Profile within a Micelle. For spherical micelles, we can obtain information about the micellar structure by determining the density profile. We calculate the site fraction distribution, s_i, of each species i (surfactant head, surfactant tail, solvent or vacancy) at a distance r from the center of mass of the micelle using

$$\langle s_i(r) \rangle = \langle N_i(r) \rangle / N_T(r)$$

where $N_i(r)$ is the number of site of species i and N_T the total number of sites at the distance r from the micelle center of mass. The density profile is obtained by ensemble averaging the site fraction distributions for micelles whose aggregation number equals the mean aggregation number ±1. Considering a bigger range of aggregation numbers for the calculation leads to a broad distribution that is not typical of the micelles formed at a given CO_2 density and temperature.

Micelle−Micelle Contact Factor. At low CO_2 density, the CO_2/surfactant systems undergo phase separation into a CO_2-rich phase and a surfactant-rich phase. In Figure 3a, we show a snapshot of an equilibrated system at $\rho_r = 1.3$, $X_S = 0.0065$, and $T = 330$ K, which shows several micelles packed together and clearly indicates phase separation. However, reference to the corresponding size distribution (Figure 3b) gives no hint of macroscopic phase separation. To help locate the conditions at which phase separation occurs, we calculate the micelle−micelle contact factor (C_{MM}), which is defined to be the number of contacts that the surfactant tails in one micelle experience with surfactant tails on surrounding micelles. A contact is counted each time that one surfactant tail unit of a micelle has a nearest or next-nearest-neighbor contact with a surfactant tail unit from another micelle. This factor is averaged over all micelles in the simulation box during the course of a simulation.

In Figure 4, the micelle−micelle contact factor (C_{MM}) is displayed as a function of CO_2 reduced density (ρ_r) for H_4T_5 surfactants in $scCO_2$ at two surfactant mole fractions: 0.002 and 0.0065. The micelle−micelle contact factor, C_{MM}, decreases strongly with increasing CO_2 reduced density up to $\rho_r = 1.5$ and then reaches a plateau

(44) Rajagopalan, R.; Rodriguez-Guadarrama, L. A.; Talsania, S. K. In *Handbook of Microemulsion Science and Technology*; Kumar, P., Mittal, K. L., Eds.; Dekker: New York, 1999; pp 105−137.

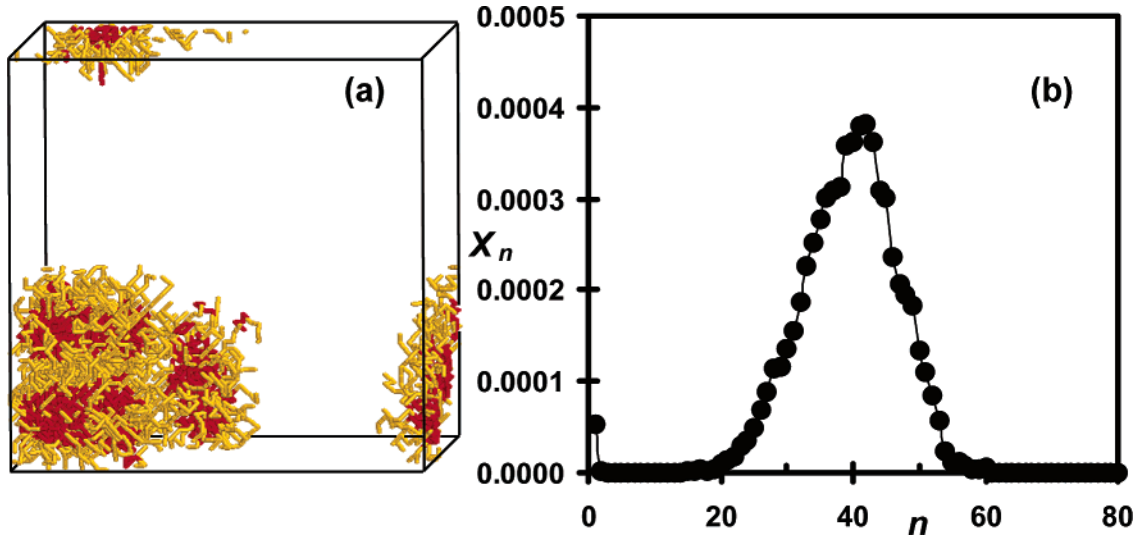

Figure 3. (a) Simulation snapshot of the final configuration for H_4T_5 surfactants in $scCO_2$ at $\rho_r = 1.3$, $X_S = 0.0065$, and $T = 330$ K. Surfactant heads are red, surfactant tail are tan, and CO_2 and vacancy sites are left blank for ease of viewing. (b) Mole fraction of surfactant (X_n) vs aggregation number (n) for this system.

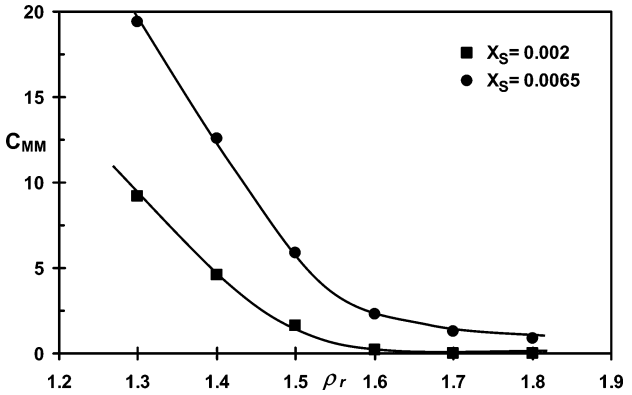

Figure 4. Micelle−micelle contact factor (C_{MM}) vs CO_2 reduced density (ρ_r) for H_4T_5 surfactants in $scCO_2$ at $X_S = 0.002$ (■) and $X_S = 0.0065$ (●) at $T = 330$ K.

at $\rho_r \geq 1.6$. The difference between the C_{MM} values at the two surfactant mole fractions is due to the increased number of micelles at the higher surfactant mole fraction which translates into a higher possibility of contact between micelles. Although the phase boundary is likely to occur just prior to the CO_2 reduced density at which C_{MM} reaches a plateau, the CO_2 reduced density when the phase transition occurs cannot be located precisely. Visual observation of snapshots corresponding to systems at $\rho_r = 1.3$ and 1.4 confirms a phase separation, but further investigation is needed to pinpoint the location of the cloud curve.

III. Results and Discussion

We have divided the results into two sections. In the first section, we consider the effect of varying the surfactant concentration on the micellar size and shape at constant CO_2 density ($\rho_r = 1.8$). In the second section, we present the phase diagram in the surfactant concentration−CO_2 density space and consider the effect of varying the CO_2 density on the cmc and the micellar size, shape, and structure. In both sections, we compare our results with previous simulation results and with experimental results when available.

III.1. Effect of Surfactant Concentration. Here, we describe the results of MC simulations of H_4T_5 surfactants in $scCO_2$ at $\rho_r = 1.8$, surfactant mole fractions $X_S = 0.002$, 0.00275, 0.0035, 0.005, and 0.0065, and $T = 330$ K. The free surfactant mole fraction (X_S^f) as a function of the total surfactant mole fraction (X_S) is shown in Figure 1. As explained in section II.4, the resulting cmc is $X_{cmc} = 0.00215$. At concentrations higher than the cmc, we note a decrease in the free surfactant concentration consistent with simulation results.[23,27,36] Table 2 summarizes properties of interest, including the mole fractions of free surfactant and micelle, the mean aggregation number, and the mean radii of gyration for the micelle and for the micellar core when $n = 25$, at each of the simulation points on Figure 1. In Figure 2 is shown the distribution of aggregation numbers associated with each of the simulation points on Figure 1. The aggregation number distribution for the concentration close to but slightly below the cmc ($X_S = 0.002$, solid line) appears to be broader and centered at lower aggregation numbers than those at concentrations above the cmc. Moreover, a comparison of the free surfactant mole fraction, X_S^f, and the mole fraction of micelles, X_{mic} (see Table 2), at this concentration ($X_S = 0.002$) and the next higher one ($X_S = 0.00275$) reveals almost no difference in X_S^f ($\Delta X_S^f = 0.00001$) while the difference in X_{mic} is comparatively significant ($\Delta X_{mic} = 0.0004$). We then deduce that the peak in the aggregation number distribution of the system at $X_S = 0.002$ is mainly due to the presence of small aggregates rather than micelles. This lends credence to our choice for the cmc definition since defining the cmc as the first concentration at which a maximum in the aggregation number distribution appears,[42] would make the system at $X_S = 0.002$ a micellar system. We also note from Table 2 that above the cmc, X_{mic} increases with the total surfactant mole fraction, X_S, while the mean aggregation number, N_a,

Table 2. Mole Fractions of Free Surfactant (X_S^f) and Micelle (X_{mic}), Mean Aggregation Number (N_a), and the Mean Radii of Gyration for the Micelle ($R_{n=25}$) and for the Micellar Core ($R_{c(n=25)}$) at $n = 25$ for five mole fractions of H_4T_5 surfactant (X_S) in supercritical CO_2 ($T = 330$ K, $\rho_r = 1.8$)

X_S	X_S^f	X_{mic}	N_a	$R_{n=25}$	$R_{c(n=25)}$	$(R - R_c)_{n=25}$
0.002	0.00105	0.00053	24.6	2.67	1.52	1.15
0.00275	0.00104	0.0013	25.5	2.67	1.52	1.15
0.0035	0.00099	0.0021	25.1	2.68	1.52	1.16
0.005	0.00093	0.0037	25.7	2.68	1.52	1.16
0.0065	0.00083	0.0053	25.9	2.68	1.52	1.16

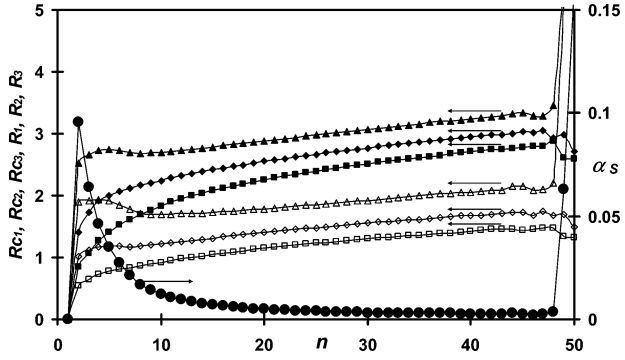

Figure 5. Three principal radii of gyration for the micelle R_1 (■), R_2 (◆), and R_3 (▲) and for the micellar core R_{c1} (□), R_{c2} (◇), and R_{c3} (△) and asphericity parameter α_S (●) vs aggregation number n for H_4T_5 surfactants in $scCO_2$ at $X_S = 0.0065$, $\rho_r = 1.8$, and $T = 330$ K.

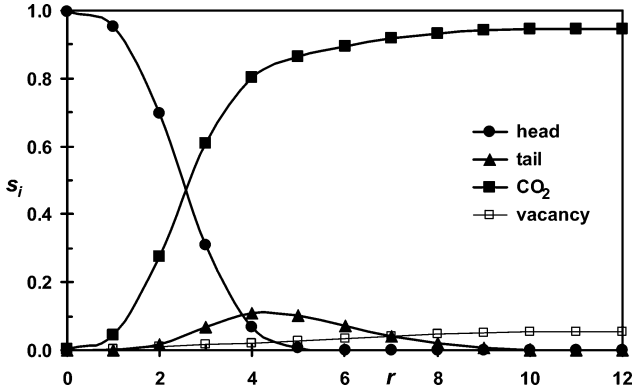

Figure 6. Density profile within a micelle for H_4T_5 surfactants in $scCO_2$ at $X_S = 0.0065$, $\rho_r = 1.8$, and $T = 330$ K plotted as site fractions s_i of surfactant head (●), surfactant tail (▲), CO_2 (■), and vacancy (□) vs the distance r from the center of mass of the micelle.

remains almost constant and approximately equal to 25 ± 1. The addition of surfactants leads then to an increase in the number of micelles but does not change the micellar size. Similar observations have been made in the literature[21,23,36] for a surfactant concentration range slightly higher than the cmc.

In Figure 5 the principal radii of gyration are shown for the micelle (R_1, R_2, R_3) and for the micellar core (R_{c1}, R_{c2}, R_{c3}), together with the asphericity parameter (α_S) as a function of the aggregation number (n) for H_4T_5 surfactants in $scCO_2$ at the highest surfactant concentration, $X_S = 0.0065$. We observe that R_1, R_2, and R_3 are of the same order of magnitude and α_S is smaller than 0.1 indicating that the micelles are roughly spherical. Similar plots at lower surfactant mole fractions exhibit the same behavior. As expected, the micelles are spherical in the surfactant concentration range considered in this work. It has been shown that elongated micelles form at concentrations that are about 10 times higher than the cmc.[12]

Another aspect of interest is the effect of overall surfactant concentration on the micellar shape. The mean radii of gyration for the micelle (R), for the micellar core (R_c), and for the micellar corona ($R - R_c$) at $n = 25$ are listed in Table 2. These remain constant as the surfactant concentration increases. This result is expected since the micellar size also remains constant over this surfactant concentration range. We believe that the mean radii of gyration for the micelle and for the micellar corona at $X_S = 0.002$ and 0.00275 are slightly lower than at higher surfactant concentrations because the principal radii of gyration are averaged over all the aggregates ($n \neq 1$) and the mole fraction of small aggregates ($1 < n \leq 5$) for systems at the low surfactant concentrations is higher. Since the mean radii of gyration for the micelle, for the micellar core, and for the micellar corona do not vary with increasing surfactant concentration, it is more accurate to calculate the principal radii of gyration at the highest surfactant mole fraction where the mole fraction of small aggregates is the lowest.

To complete the description of the H_4T_5 surfactant/CO_2 systems at $\rho_r = 1.8$ and $T = 330$ K, we report the density profile within micelles of size $n = 25 \pm 1$. Because the density profile does not depend on the surfactant concentration,[23] we consider only one surfactant mole fraction, that is $X_S = 0.0065$. In Figure 6 we display the site fractions of surfactant head, surfactant tail, solvent, and vacancy at a distance r from the center of mass of the micelle. As expected, the micellar core consists mainly of surfactant heads. The density of CO_2 sites increases with r. Considering that the density of CO_2 sites is higher than the density of surfactant head sites ($s_C \geq s_H$) at $r \geq 2.5$, we take this distance as the inner limit for the core−corona interface. At $r = 4$, the density of surfactant tail sites reaches a maximum which is higher than the density of surfactant head sites ($s_T \geq s_H$), marking the outer limit for the core−corona interface. Therefore, the core−corona interface is broadly extended from $r = 2.5$ to $r = 4$ and contains all of the system components, i.e., surfactant head, surfactant tail, and CO_2. Finally, the micellar corona consists of surfactant tails highly solvated by CO_2 and some vacancy sites. Surfactant tails are not found at $r \geq 10$. Our observations of the micellar structure are consistent with observations made in other simulation studies.[23,35,38] However, in our work, we note that the core−corona interface extends further into the micellar core. We believe that this is due to the mild repulsive interaction parameter w_{CH}, which allows the penetration of CO_2 into the micellar core.

III.2. Effect of Varying CO_2 Density. To study the effect of varying CO_2 density on the system properties, we performed additional MC simulations of H_4T_5 surfactants in $scCO_2$ at $\rho_r = 1.3$, 1.4, 1.5, 1.6, and 1.7, $X_S = 0.002$, 0.0035, 0.005, and 0.0065, and $T = 330$ K. The mole fractions of free surfactant (X_S^f) and micelle (X_{mic}) and the mean aggregation numbers (N_a) are calculated at the four surfactant mole fractions studied for each CO_2 density in order to determine the cmc. For $\rho_r = 1.3$, simulations are only performed at $X_S = 0.002$ and $X_S = 0.0065$; no cmc is determined. The free surfactant mole fractions (X_S^f) and the mean aggregation number (N_a) at all conditions considered are listed in Table 3.

The resulting phase diagram, plotted in X_S−ρ_r space, is shown in Figure 7a. The diagram exhibits three regions: (1) a two-phase region at low CO_2 reduced density ($\rho_r \leq 1.4$) where the surfactant molecules phase separate from the CO_2; (2) a micellar region at high CO_2 reduced density ($\rho_r \geq 1.4$) and high surfactant mole fraction where the surfactants form micelles; (3) a free surfactant region at high CO_2 reduced density ($\rho_r \geq 1.4$) and low surfactant mole fraction where the surfactants are completely solubilized by CO_2. Our phase diagram is in good qualitative agreement with the experimental phase diagram for PVAC-*b*-PTAN in CO_2 at $T = 318$ K[45] (Figure 7b). As discussed in section II.4, a two-phase region is apparent at CO_2 reduced densities $\rho_r = 1.3$ and 1.4 (based on visualization of the simulation box) but the boundary of

(45) Taylor, D. K.; Keiper J. S.; DeSimone, J. M. Polymer Self-Assembly in Carbon Dioxide. *Ind. Eng. Chem. Res.* **2002**, *41* (18), 4451−4459.

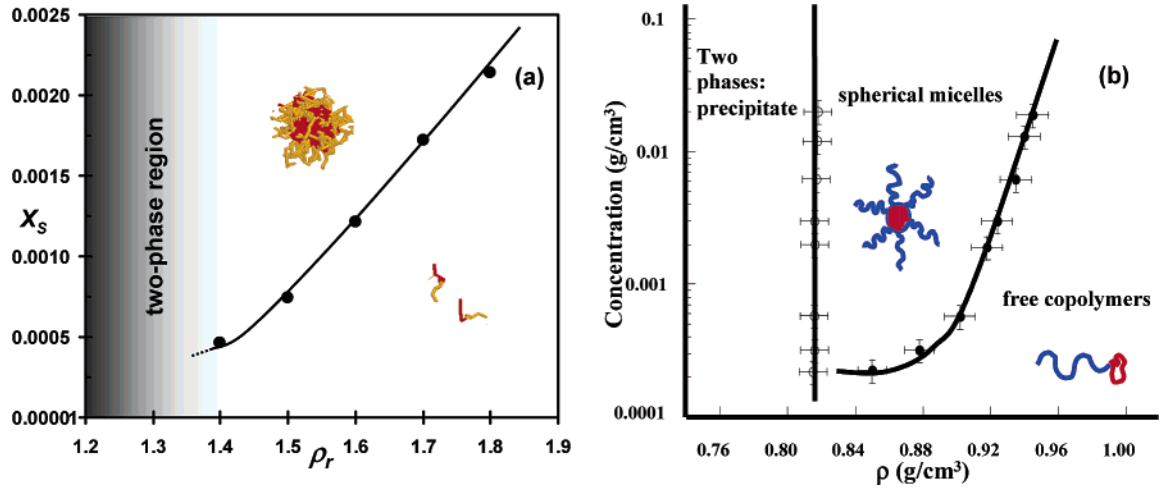

Figure 7. (a) Phase diagram plotted as surfactant mole fraction (X_S) vs CO_2 reduced density (ρ_r) for H_4T_5 surfactants in $scCO_2$ at $T = 330$ K. The diagram exhibits a two-phase region (dark area) and the cmc curve (●) that divides the free surfactants region (low concentration) from the micellar region (high concentration). (b) Phase diagram plotted as surfactant concentration vs CO_2 density for the PVAC-*b*-PTAN surfactant at $T = 318$ K. (Reproduced with permission from ref 45.)

Table 3. Mole Fractions of Free Surfactant (X_S^f) and Mean Aggregation Numbers (N_a) for Four Surfactant Mole Fractions (X_S), at Six CO_2 Densities (ρ_r) and at $T = 330$ K

	X_S^f				N_a			
ρ_r	$X_S = 0.002$	$X_S = 0.0035$	$X_S = 0.005$	$X_S = 0.0065$	$X_S = 0.002$	$X_S = 0.0035$	$X_S = 0.005$	$X_S = 0.0065$
1.3	0.0001			0.00009	42.5			42.6
1.4	0.00021	0.00021	0.00019	0.00017	42	47.1	41.3	42.1
1.5	0.00037	0.00032	0.00033	0.00029	39.5	37.6	40	39.5
1.6	0.00059	0.00058	0.00056	0.00050	35.1	36.2	37.1	35.5
1.7	0.00085	0.00081	0.00077	0.00070	30.1	30.4	30.4	30.5
1.8	0.001	0.00099	0.00093	0.00083	24.7	25.1	25.7	25.9

the two-phase region cannot be located precisely. For this reason, the two-phase region in Figure 7a is represented by a shaded area but the cloud curve is not traced. In Figure 7a, the simulation points represent the cmc calculated at each CO_2 reduced density following the methodology described in section II.4. The cmc curve marks the micelle-to-free surfactant transition separating the micellar region from the free surfactant region. We note an increase in the cmc with CO_2 density, consistent with experimental observations on PVAC-*b*-PTAN in CO_2 at $T = 318$K[46] and PFOA-*b*-PVAC in CO_2 at $T = 338$ K.[47]

The percentages of free surfactants (P_{free}) and of surfactants forming micelles (P_{mic}) as a function of CO_2 reduced density are plotted in Figure 8. We observe an increase in the percentage of free surfactants and a decrease in the percentage of surfactants forming micelles with increasing CO_2 density for all the surfactant mole fractions. For the system at $X_S = 0.002$ and $\rho_r = 1.8$, the percentage of free surfactants is higher than 50% which is a characteristic of a system below the cmc. The general behavior, depicted in Figure 8 with increasing CO_2 density, is consistent with the increased surfactant solubility in CO_2, which is, in fact, the origin of the micelles-to-free surfactant transition occurring at the critical micelle density (cmd).[48]

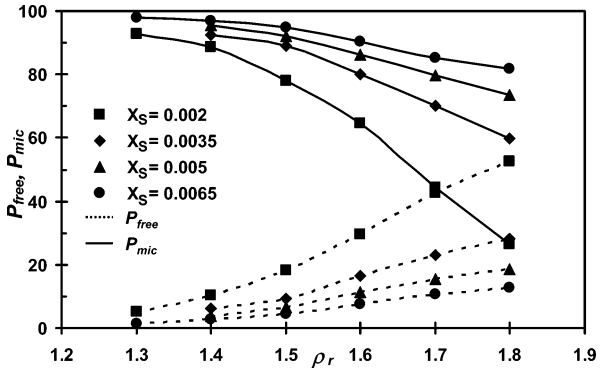

Figure 8. Percentages of free surfactants (P_{free}) and of surfactants forming micelles (P_{mic}) vs CO_2 reduced density (ρ_r) for H_4T_5 surfactants in $scCO_2$ at $X_S = 0.002$ (■), 0.0035 (◆), 0.005 (▲), and 0.0065 (●) at $T = 330$ K.

To investigate the effect of varying CO_2 density on the micellar size, we plot the mean aggregation number (N_a) as a function of CO_2 reduced density (ρ_r) for H_4T_5 surfactants in $scCO_2$ at two surfactant mole fractions (0.002 and 0.0065) in Figure 9. The mean aggregation number is constant in the two-phase region ($\rho_r \leq 1.4$) and then decreases as the CO_2 reduced density increases. The decrease in the mean aggregation number with increasing CO_2 density is consistent with experiments on PS-*b*-PFOA in CO_2 at $T = 338$ K,[11] PVAC-*b*-PTAN in CO_2 at $T = 318$ K,[46] PFOA-*b*-PVAC in CO_2 at $T = 338$ K,[47] and PFOA-*g*-PEO in CO_2 at $T = 333$ K.[49] This trend can be explained

(46) Buhler, E.; Dobrynin, A. V.; DeSimone, J. M.; Rubinstein, M. Light-Scattering of Diblock Copolymers in Supercritical Carbon Dioxide: CO_2 Density-Induced Micellization Transition. *Macromolecules* **1998**, *31*, 7347−7355.

(47) Zhou, S.; Chu, B. Laser light scattering study of pressure-induced micellization of a diblock copolymer of poly(1,1-dihydroperfluorooctyl-acrylate) and poly(vinyl acetate) in supercritical carbon dioxide. *Macromolecules* **1998**, *31*, 5300−5308.

(48) Triolo, R.; Triolo, A.; Triolo, F.; Steytler, D. C.; Lewis, C. A.; Heenan, R. K.; Wignall, G. D.; DeSimone, J. M. Structure of diblock copolymers in supercritical carbon dioxide and critical micellization pressure. *Phys. Rev. E* **2000**, *61*, 4640−4643.

(49) Fulton, J. L.; Pfund, D. M.; McClain, J. B.; Romack, T. J.; Maury, E. E.; Combes, J. R.; Samulski, E. T.; DeSimone, J. M.; Capel, M. Aggregation of Amphiphilic Molecules in Supercritical Carbon Dioxide: A Small-Angle X-ray Scattering Study. *Langmuir* **1995**, *11*, 4241−4249.

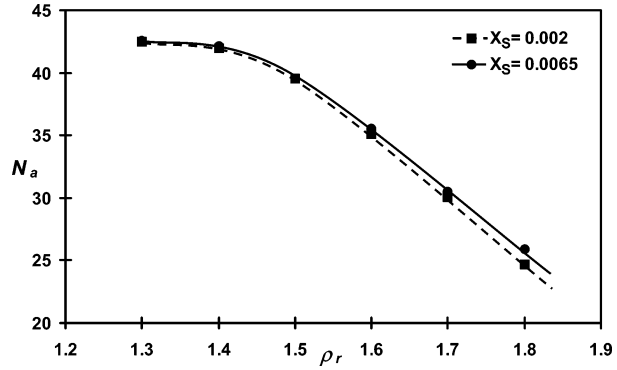

Figure 9. Mean aggregation number (N_a) vs CO_2 reduced density (ρ_r) for H_4T_5 surfactants in $scCO_2$ at $X_S = 0.002$ (■) and $X_S = 0.0065$ (●) at $T = 330$ K.

by the increase in solvent quality of CO_2 with CO_2 density[46] which hinders micellization and the formation of large micelles.[31] We also note that there is a small difference in the mean aggregation numbers for the two surfactant mole fractions at constant CO_2 density and that this difference increases with CO_2 density. From the above observations, it appears that the CO_2 solvating ability has a strong effect on the micellar size. Although direct quantitative comparison between our result on micellar size and experiment would be interesting, this is not possible because the model surfactant used in this work does not mimic any specific surfactant. We can say, however, that the aggregation numbers calculated here are not outside of the range of aggregation numbers estimated by scattering studies, i.e., from fewer than 10[11,48,49] to 120[46,49] surfactants, depending on the surfactant nature and concentration, and on the CO_2 density.

To evaluate the effect of varying CO_2 density on the micellar shape, we study the variation of the principal radii of gyration with the aggregation number. The plots of the principal radii of gyration as a function of the aggregation number at $X_S = 0.0065$ for each CO_2 density (data not shown) exhibit the same behavior as in Figure 5, that is, R_1, R_2, and R_3 are of the same order of magnitude and α_S is smaller than 0.1. This is typical of spherical micelles in agreement with scattering studies on PS-*b*-PFOA,[11] PVAC-*b*-PTAN,[46,48] and PFOA-*g*-PEO in CO_2.[49] The mean radii of gyration at $X_S = 0.0065$ and $\rho_r = 1.4$, 1.5, 1.6, 1.7, and 1.8 for the micelle (R), for the micellar core (R_c), and for the micellar corona ($R - R_c$), as a function of the aggregation number (n) are presented in parts a, b, and c of Figure 10, respectively. For ease of viewing, we only show the results in the range of aggregation number (n) that includes the mean aggregation numbers (N_a) of the systems studied. As seen in Figure 9, this range is $20 \leq n \leq 45$. The increase in the mean radius of gyration for the micelle with increasing CO_2 density (Figure 10a) appears to be due mainly to an increase in the mean radius of gyration for the micellar corona (Figure 10c) since the mean radius of gyration for the micellar core remains almost constant (Figure 10b). The increase in the mean radius of gyration for the micellar corona with increasing CO_2 density can be explained by realizing that the surfactant tails extend further into the solvent due to the increased solubility of surfactants with increasing CO_2 density. This extension of the surfactant tail with CO_2 density plays an important role in the stabilization of microemulsion and emulsion droplets in CO_2/surfactant/water systems. The mean radii of gyration for micelles of size N_a and for their micellar core at $X_S = 0.0065$ for each CO_2 density are summarized in Table 4. The decrease in the mean radii of gyration for the micelle and for the

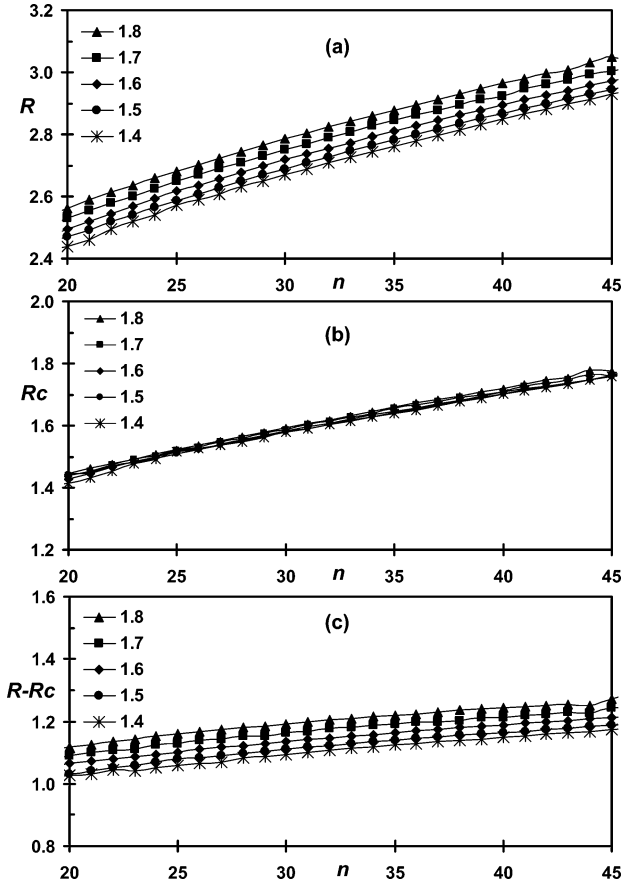

Figure 10. Mean radii of gyration for (a) the micelle (R), (b) the micellar core (R_c), and (c) the micellar corona ($R - R_c$) vs aggregation number n for H_4T_5 surfactants in $scCO_2$ at $X_S = 0.0065$, with ρ_r ranging from 1.4 to 1.8 and $T = 330$ K.

Table 4. Mean Aggregation Number (N_a) and Mean Radii of Gyration for the Micelle (R) and for the Micellar Core (R_c) for Five CO_2 Densities (ρ_r) at $X_S = 0.0065$ and at $T = 330$ K

ρ_r	N_a	R	R_c
1.4	42.1	2.88	1.72
1.5	39.5	2.86	1.70
1.6	35.5	2.82	1.65
1.7	30.5	2.76	1.60
1.8	25.9	2.70	1.54

micellar core with increasing CO_2 density is consistent with the experimental trend displayed in the experimental studies mentioned earlier.[11,49]

The effect of varying CO_2 density on the micellar structure can be further understood by plotting the density profile within micelles of similar size $n = 35 \pm 1$ at several CO_2 reduced densities and $X_S = 0.0065$. The aggregation number $n = 35$ is chosen because the mole fraction of surfactant forming micelles of this size at all CO_2 densities is $X_n \geq 0.0001$. Because the density profiles exhibit similar variation to that shown in Figure 6, only the site fractions of surfactant head, surfactant tail, and CO_2 in the range $0 \leq s_i \leq 0.5$ at $\rho_r = 1.4$, 1.6, and 1.8 are displayed in Figure 11 as a function of the distance r from the center of mass of the micelle. It appears that the structure of the micellar core and the core−corona interface ($r \leq 4$) do not change while the structure of the micellar corona close to the core−corona interface ($4 \leq r \leq 6$) is slightly altered with increasing CO_2 density. In effect, the decrease in the density of surfactant head sites and the increase in the density of CO_2 sites with increasing distance r are virtually the same for the three CO_2 reduced densities. Moreover,

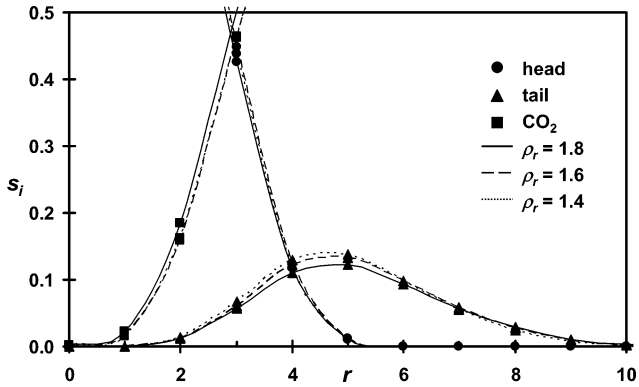

Figure 11. Density profile within a micelle for H_4T_5 surfactants in $scCO_2$ at $n = 35 \pm 1$, $X_S = 0.0065$, $\rho_r = 1.4$ (dotted line), 1.6 (dashed line), and 1.8 (solid line), and $T = 330$ K, plotted as site fractions s_i of surfactant head (●), surfactant tail (▲), and CO_2 (■) vs the distance from the center of mass of the micelle r.

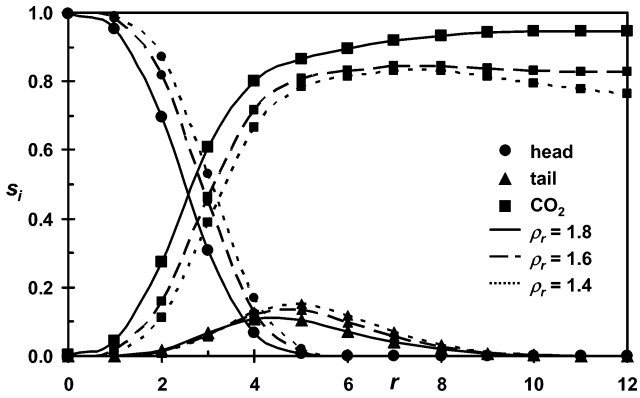

Figure 12. Density profile within a micelle for H_4T_5 surfactants in $scCO_2$ at $X_S = 0.0065$, $\rho_r = 1.8$ (solid line), 1.6 (dashed line), and 1.4 (dotted line), and $T = 330$ K plotted as site fractions s_i of surfactant head (●), surfactant tail (▲), and CO_2 (■) vs the distance from the center of mass of the micelle r.

regardless of the system CO_2 density, the lower limit for the core−corona interface, corresponding to the distance at which $s_C \leq s_H$, is still at $r = 3$ and the upper limit, corresponding to the distance at which $s_T \geq s_H$, is still at $r = 4$. Finally, the maximum in the density of surfactant tail sites found close to the core−corona interface, decreases with increasing CO_2 density consistent with the extension of the surfactant tail into the CO_2 with increasing CO_2 density.

Additionally, we plot the density profile within micelles of size $N_a = 42$, 35, and 25 at CO_2 reduced densities $\rho_r = 1.4$, 1.6, and 1.8, respectively, and $X_S = 0.0065$, to gain insight into the combined effect of varying CO_2 density and micellar size on the micellar structure (Figure 12). For ease of viewing, the vacancy site fraction is not shown. Because the variation of CO_2 density does not affect the structure of the micellar core and the core−corona interface at fixed micellar size (see Figure 11), the following observations can be made concerning the variation of the micellar structure with increasing micellar size. The micellar core becomes bigger as the micellar size increases since the lower and upper limits for the core−corona interface move to larger values of the distance r. The micellar corona does not seem to be affected by the increase in micellar size.

IV. Summary

In this work, lattice-based Monte Carlo simulations are performed to study the effect of varying the surfactant concentration and CO_2 density on the phase behavior of surfactants in supercritical CO_2. We first determine the cmc and the micellar size, shape, and structure at constant CO_2 density. The trend of free surfactant concentration with total surfactant concentration, the presence of spherical micelles of constant size over the surfactant concentration range studied, and the results for the micellar structure are all consistent with previous simulation studies of incompressible systems.[21,23,28,36]

We have also examined how the increased solvating ability of CO_2 as CO_2 density increases affects the properties of $scCO_2$/surfactant systems. The complete phase diagram in surfactant mole fraction versus CO_2 reduced density space is in qualitative agreement with experimental phase diagrams for different surfactants in CO_2 available in the literature.[11,46,47,49] Although the results for the micelle−micelle contact factor do not allow the exact determination of the cloud curve at low CO_2 density, we can distinguish between a two-phase region and a micellar region by visualizing the simulation box. We find an increase in the cmc and a decrease in the micellar size and in the percentage of surfactants forming micelles with increasing CO_2 density. These results are consistent with the experimentally observed trend that surfactant solubility in CO_2 increases as CO_2 density increases. Evaluation of the principal micelle radii of gyration indicates that the micelles are spherical throughout the surfactant concentration−CO_2 density space studied. The increase in the mean radius of gyration for the micellar corona with increasing CO_2 density is explained by the extension of the surfactant tails into the solvent. Finally, the variations of the micellar density profile upon increasing CO_2 density and decreasing micellar size indicate that the extension and structure of the micellar core depend solely on the micellar size but that the extension and structure of the micellar corona are strongly affected by the CO_2 density.

To our knowledge, these are the first lattice Monte Carlo simulations to reproduce the experimental trends found for $scCO_2$/surfactant systems with CO_2 density. We have shown that a simple model can also provide considerable insight into the effect of CO_2 density on the solvent quality and, hence, on the behavior of surfactants in such solvents.

The simplicity of our molecular model compared to real supercritical CO_2/nonionic surfactant systems prevents a direct quantitative comparison with experiment. In effect, most of the surfactants used in supercritical CO_2 systems are polydispersed block copolymers containing bulky and complex fluorine- or silicone-containing units while our model surfactants consist of a fixed number of same size units. Although the interaction energy parameters in our model could in principle be obtained by fitting the solubility curves of the two homopolymers constituting the surfactant, and of the surfactant itself, more precisely tuned interaction energies might not be able to overcome the limitations associated with our simple treatment of the steric effect and our neglect of surfactant polydispersity.

Acknowledgment. The material is based upon work supported by the STC Program of the National Science Foundation under Agreement No. CHE-9876674. Acknowledgment is made to the donors of the Petroleum Research Fund administered by the American Chemical Society and the Department of Energy (Grant No. DE-FG02-97-ER14771). We thank the National Partnership for Advanced Computational Infrastructure (Grant npa205) for providing supercomputer time.

LA0347760